



# Experimental and numerical investigation of flow patterns in symmetrical spurs

Ali Yıldız <sup>a,\*</sup>, Alpaslan Yarar <sup>a</sup>, Mehmet Ali Hınıs <sup>b</sup>, G. Elif Yarbaşı Kayhanlar <sup>a</sup>

<sup>a</sup> Konya Technical University, Civil Engineering Department, Konya and 42250, Turkey

<sup>b</sup> Aksaray University, Civil Engineering Department, Aksaray and 68100, Turkey

## Abstract

Spurs are hydraulic structures used to protect riverbanks from erosion and to concentrate the flow on the river axis. As the flow approach the spurs, discontinuous in the streamlines are occurred and vortices form before the spurs. In previous studies, spurs were generally placed on a one side of the open channel, and the vortices on the upstream and downstream were investigated. In this study, the changing flow velocities, and flow patterns on the upstream side of two spurs which are placed opposite each other on both side of the open channel were investigated. Spurs have same geometric parameters and placed with 90° the side wall angle. For 2 different discharge values ( $Q=17.66$  lt/sn and  $Q=15.27$  lt/sn), 3-Dimensional velocity measurements were made with ADV (Acoustic Doppler Velocimetry) at 20 different points on the upstream side of the spurs. With these obtained velocity profiles, flow patterns are investigated. Velocity values obtained from the numerical model give consistent velocity values with experiments and the maximum value of the margin of error between the models did not exceed 9%. In the experiments, the highest and lowest velocity values were measured as 3.2 cm/s and 88 cm/s, respectively. Unlike spurs placed at one side of the channel, no vortex was observed on the upstream side of the spurs in the experiments.

**Keywords:** Flow patterns; numerical modelling; open channel; spur

## 1. Introduction

Flow regulation structures are built for various purposes. Some of those; protecting coastal from erosion, riverbed from scouring, preventing floods, regulating the water level in the rivers, allowing transportation, and ensuring the safety of water structures. Flow in the rivers can carry a certain amount of sediment depending on the flow conditions, and these transported sediments can cause problems in dam reservoirs and hydroelectric facilities. If the flow rate falls below a certain value, sediment accumulations are observed at the bottom of the stream, If the velocity exceeds a certain value (in case the shear stress is greater than the critical shear stress), scours are observed in the riverbed [1]. When the velocity in the dam reservoirs is close to zero, the sediments carried by the flow will settle down and cause accumulation in the reservoirs [2]. The useful life of the dams is determined by the amount of sediment carried from the basin to dam reservoir by the river. As seen from Fig 1. The sediments carried by the stream reduce the active storage volume after filling the dead volume of the dam [3]. In addition, suspended sediments are carried by flow to turbines of hydroelectric facilities can damage turbine blades [4].

\* Corresponding author. Tel.: + 905555642466.

E-mail address: ayildiz@ktun.edu.tr

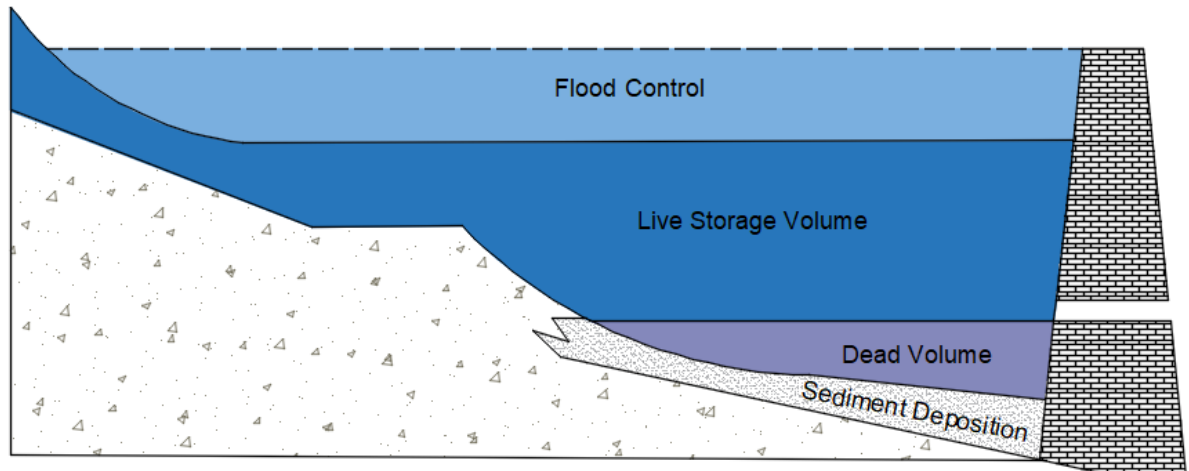


Fig 1: Volume distribution of dam reservoir

Spurs, which regulate the stream on rivers, are hydraulic structures used to protect the coast from erosion and control the siltation of sediments by diverting the flow away from the coast [5, 6]. Today, spurs are used to improve environmental conditions and capture sediments along a riverbank. There are different types of spurs depending on their permeability, flow condition and shape. A spur can be a permeable or impermeable, depending on the passage of water through it [7]. Permeable spurs are made of wood, steel or reinforced concrete piles, while impermeable spurs are manufactured as a whole from earth, stone or reinforced concrete. Depending on whether the spurs are completely submerged or partially submerged, they can be in a submerged or free flow state. They can also be in a shape of straight, T-shape, L-shapes, hockey shaped, reverse hockey shaped, flat port head, different angles to the flow [8]. The investigation of fluid behavior in a vacuum has long been an important topic in the field of fluid mechanics. These fluid behaviors are modeled with the governing equations finite element method [9]. The Boussinesq-Darcy law and the thermal instability model can be used to simulate convective heat transfer under the influence of magnetic forces in a porous medium of nanofluids [10].

While the spurs protect the coast from erosion and direct the flow, they create a certain resistance against the flow like every river structure and cause the deterioration of the streamline [2]. Disrupted streamlines create turbulence around the spur, and while these turbulences fade over time and cause sediments to settle, in some areas they can cause scour due to increased flow velocity. Many studies have been done on spurs. Özyaman [11], by changing the spur lengths and wall angles, experimentally investigated the effects of these parameters on streamlines behaviors, scour depth and scour volume. By performing nonlinear multiple regression analysis with the data obtained from the experiments, different relations giving the coefficient of resistance, scour depth and scour volume were proposed. Safarzadeh et al., [8] investigated turbulent flows around straight and T-shaped spurs. Flow velocities at the bottom of the channel were lower in T-shaped spurs than in straight spurs. Köken et al. [12] investigated the effects of spur length on horseshoe vortex system, bed shear stress and pressure using 3 different spur lengths. Some researchers have also used numerical modeling techniques to determine the hydraulic properties of spurs. Giglou et. al. [13] investigated the effects of different spur angles of 90 and 120 degrees on sedimentation. Ning et. al. [14] investigated the effect of different spur spacings on scouring.

In order to determine the sediment capture capacity of the spurs correctly, velocity distributions and vortex structures around the spurs should be determined correctly. Although velocity distributions around a spur structure to be built in a laboratory environment can be accurately determined with velocity measuring instruments, these data are difficult to detect on a spur to be built on a large river in reality. It can be determined by numerical modeling techniques, but the accuracy of these models needs to be tested and calibrated in laboratory experiments. In the previous studies, investigations were made on the vortex structures and flow velocities on the downstream side of single or serial spurs placed on one side of the channel. In this study, the upstream velocity values of two opposing spurs placed at an angle of 90° in an open channel system were measured with ADV (Acoustic Doppler Velocimetry) and eddies were investigated. The purpose of these measurements is to detect the velocity differences they cause after the spurs are placed in an open channel system and to understand the behavior of the flow patterns. In addition, numerical models of this spur system were created in one-to-one dimensions, the results obtained from the numerical model were compared with the experiments, and the accuracy of the numerical model was tested.

## 2. Materials and methods

### 2.1. Hydraulic of the spurs

There are many factors that affect sediment capture capacity of the spurs. The most important of these factors are the magnitude of the flow velocities and the behavior of the eddies caused by the spurs. An impermeable vertical wall barrier (spur) placed on one or both side walls of a freely flowing channel create an unstable, three-dimensional, highly turbulent flow field on upstream and downstream side of the spur. On the upstream side of the spurs, a distinct downflow occurs on the front face of the vertical wall barrier. Separation zones are observed both downstream and upstream of the spurs [15]. In order to design an economical, stable and hydraulically efficient spur, these velocities and eddies must be accurately determined.

As the flow approaches the spur, the flow starts to leave the wall from the upstream side of the spur. As seen from Fig 2, with the separation of the flow from the wall, eddies are formed on the upstream and downstream side of the spur. The parts where these eddies are separated from the main flow are called shear layers. The number of eddies formed after the spur may vary depending on the wall angle of the spur [16].

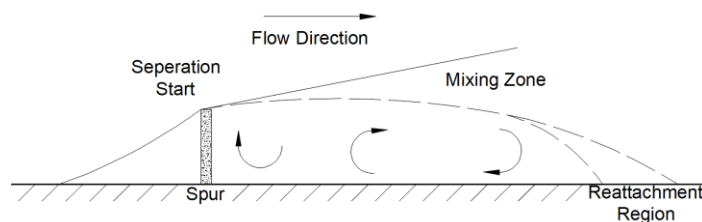


Fig 2: Flow around a spur

The location of the reattachment region varies depending on the geometric characteristics of the spur, the flow velocity, and the water depth. The separation layer, separation zone and vortices are shown in Fig 2. From the tip of the spur to the opposite channel bank is called the main flow zone. The return flow is usually located downstream of the spur with two relatively large eddies. There is a velocity difference between the main flow region and the backflow region, which leads to the formation of a shear layer between the two regions. At a certain point, the vortices are end and the flow reconnects to the main flow.

The basic geometric parameters to be considered in spur design are showed on Fig 3. A single spur or a series of spurs can be placed on one or both sides of the river to shape the spur area. Since scours at the bottom of the channel and on the shores are affected by the flow conditions directed by the spurs, therefore angle of the spur with wall has a great influence on the scour depth.

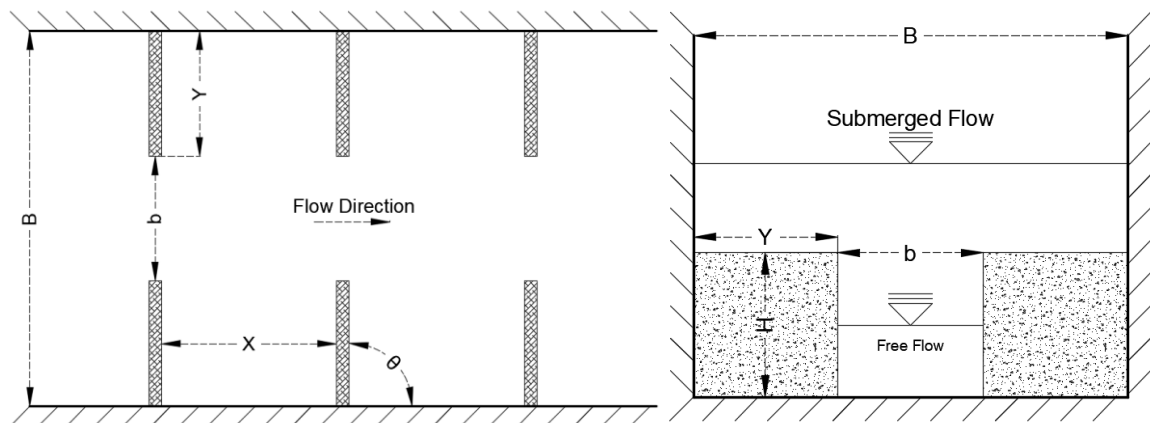


Fig 3: Top and side view of spurs and geometric parameters

Where,  $B$  is the Channel Width,  $b$  is the net opening between spurs,  $X$  is the distance between spurs,  $Y$  is the spur length,  $\theta$  is the spur angle,  $H$  is the spur height,  $N$  is the number of spurs.

## 2.2. Experimental Study

The open channel setup used in the experiments is 6.50 m long, 0.60 m wide and 0.50 m high. The flow in the open channel of the experimental setup is provided by two pumps connected in parallel to the system. The pumps send the water they receive from reservoir-1 to reservoir-2. The water coming to reservoir-2 then flows into the open channel by an opening. The amount of flow that the pumps will discharge is adjusted by the frequency changers on the panel to which the pumps are connected. Thus, the flow rate range given to the system varies between 1 and 45 lt/sn. Discharge values are read with an ultrasonic flowmeter which have 0.01 lt/sn reading sensitivity placed between the pipes after the pumps. The open channel system works with the circulation of water (Fig 4).



Fig 4: Open channel system used in experiments.

The spurs are placed 3 m away from the Reservoir-2, at the midpoint of the open channel. The purpose of choosing a point in the middle of the open channel is to not be affected by the fluctuations in the transition from the reservoir to the open channel and to obtain a smooth water surface. The length of the spurs placed on both sides of the canal is 20 cm as seen Fig 5. After the spurs are placed, a distance of 20 cm net opening remain between them for the water to pass through. The spurs are made of 1 cm thick plexiglass.

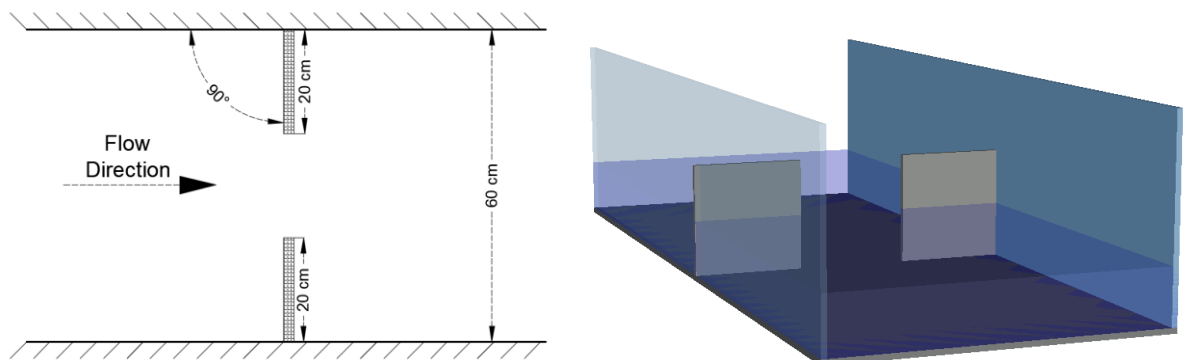


Fig 5: Spurs placed in open channel.

To understand the behavior of the vorteks systems on the upstream side of the spurs, measurements were made with the ADV device. The  $x$ ,  $y$ ,  $z$  velocities were measured for each point to determine the direction of the streamlines formed in the eddies and the magnitude of their velocities. A total of 20 points were measured with the ADV (Acoustic Doppler Velocimetry) device on the upstream side of the spurs (Fig 6). A coordinate system has been created for a clear understanding of the locations of the velocity measurement points. These 20 points are

named by numbers in columns and letters in rows. The velocity at each point was measured in 3 dimensions and  $V_x$ ,  $V_y$  and  $V_z$  velocities are determined.

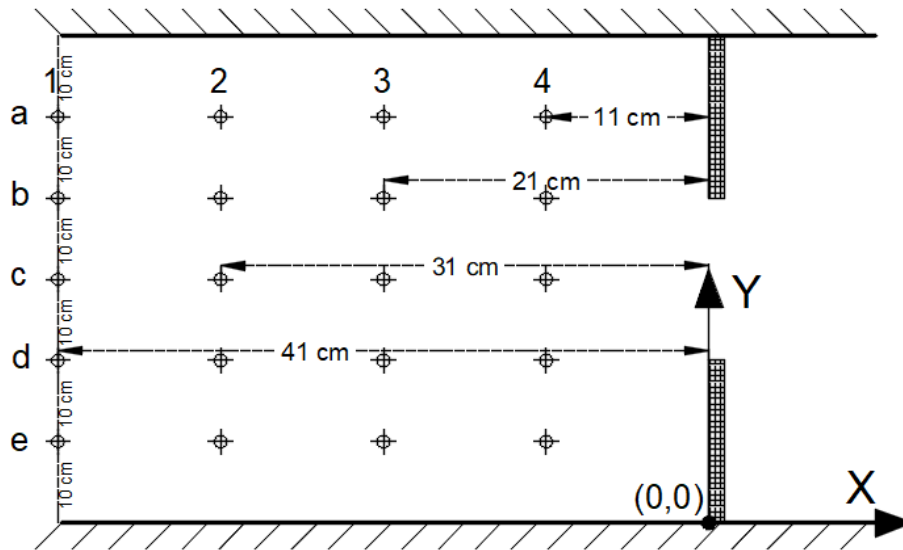


Fig 6: Coordinate system which shows measurement points.

The general diagram of the measured ADV instrument is shown in the Fig 7. Velocity measurement is the measurement of the velocity of liquids. ADV devices measure the velocity of water using a physical principle called the doppler effect. The Doppler Effect is the change in the frequency of a sound wave when a wave source moves relative to the observer or the observer himself moves relative to the wave source. Accelerometers measure velocity by transmitting a pair of short sound pulses at a given frequency into the water column. Part of the sound wave is reflected to the device; the detected return signal is processed by the device and the speed of the water is determined. The measuring volume is defined by the intersection of the three curved receivers and the central transmitter. The measurement volume for the adv used in these experiments is 5 cm from the transmitter. The reading speed values are read from this point, that is, from inside the measurement volume. It is important to determine the exact location of this measurement volume in order to know where the velocity values read belong to the flow section. In this study, the measurement volume is 7 cm above the base for a flow rate of  $Q=17.66$  lt/sn and  $Q=17.27$  lt/sn.

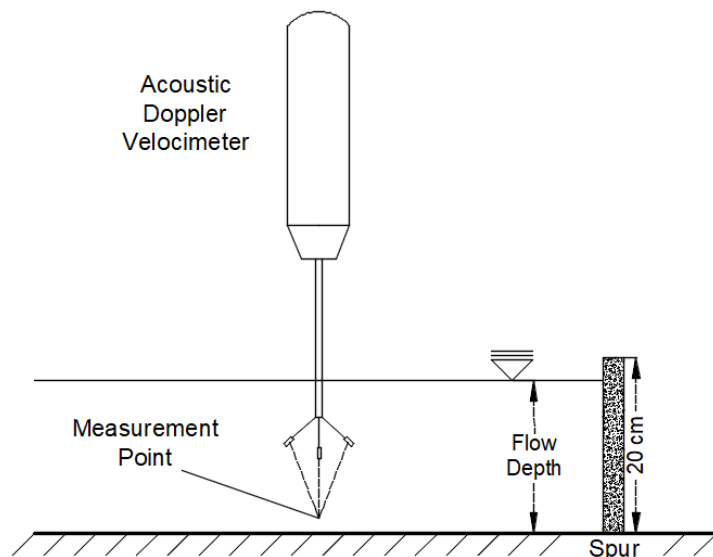


Fig 7: ADV device used for velocity measurement.

### 2.3. Numerical Modelling

Numerical modelling is an engineering discipline in which mathematical and numerical methods are used to model and simulate the behavior of fluids (liquids, gases or mixtures). Numerical modelling is a powerful tool for analyzing and optimizing the movement and interaction of fluids in real-world applications. As in this study, numerical modelling is used for modeling the movement of water in an open channel. However, numerical modelling techniques are also used for modeling non-Newtonian fluids such as blood in the human body [17, 18]. Additionally, numerical modelling techniques are used for the modeling of nanofluids containing nanoparticles [19, 20].

The numerical models of the experiments were made with the Fluent program of ANSYS. ANSYS-Fluent can solve fluid problems involving liquid-solid, liquid-gas, liquid-solid-gas and gas-solid interactions. It uses mixture, Eulerian, volume of fluid (VOF) and discrete phase models to solve these problems. Navier-Stokes equations for numerical modeling of fluids are often expressed as quadratic partial differential equations obtained by segmenting a field. The Navier-Stokes equations are the basic equations that describe fluid motion. These equations are used to determine the conservation of momentum and the behavior of the fluid. These equations are solved by dividing the computational space into meshes and solving the equations on mesh. Usually, the discrete form of the equations is obtained using the finite difference, finite element, or finite volume methods.

Equations used for solving differential equation sets derived from momentum, energy and mass conservation laws;

The equation for conservation of mass, or continuity equation, can be written as Equation-1:

$$\frac{\partial \rho}{\partial t} + \rho(\nabla \times \vec{v}) = 0 \quad (1)$$

For 2D axisymmetric geometries, the continuity equation is given by Equation-2:

$$\frac{\partial \rho}{\partial t} + \frac{\partial}{\partial x}(\rho v_x) + \frac{\partial}{\partial r}(\rho v_r) + \frac{\rho v_r}{r} = 0 \quad (2)$$

Conservation of momentum in an inertial (non-accelerating) reference frame is described by Equation-3:

$$\frac{\partial}{\partial t}(\rho \vec{v}) + \nabla \times (\rho \vec{v} \vec{v}) = -\nabla P + \nabla \times (\vec{\tau}) + \rho \vec{g} + \vec{F} \quad (3)$$

where,  $\nabla$  is the gradient operator,  $x$  is the axial coordinate,  $r$  is the radial coordinate,  $\vec{v}$  is the velocity,  $v_x$  is the axial velocity,  $v_r$  is the radial velocity,  $\rho$  is the density of fluid,  $P$  is the static pressure,  $g$  is the gravity,  $\vec{F}$  is the body force and  $\vec{\tau}$  is the viscous stress tensor.

#### 2.3.1. Geometry

3D numerical models were created with the same dimensions and environmental conditions as the experimental setups. In the Fluent program, the analysis is done in the solid volume instead of the flow volume. Flow volume is the volume of the outside of solid surfaces where water and air can be found. The flow volumes to be analysed were created to be consistent with the solid volumes. The flow volumes to be used in the analysis were created in AutoCAD and transferred to the program in .sat (Standard ACIS Text) format. The dimensions of the flow volume used in the analysis are 100 cm x 60 cm x 25 cm and is seen Fig 8.

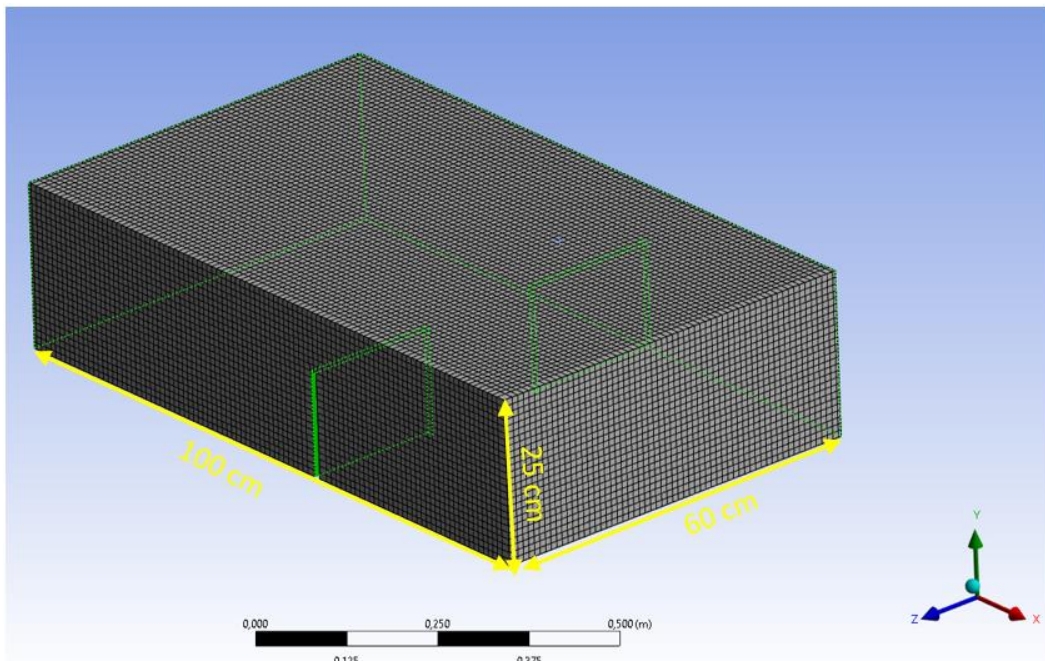


**Fig 8: Flow volume used in numerical modelling.**

### 2.3.2. Mesh

To apply the finite volume method, this flow volume must be divided into meshes. In each mesh inside the flow volume, the continuity (Navier-Stokes) equation is solved. As the number of meshes contained in the flow volume increases, the sensitivity of the solution also increases. Since the geometry of the flow volume of the numerical model is a rectangular prism, the shape of the meshes is also chosen as a cube and cartesian mesh was used. The edge size of the cube-shaped meshes used is 0.02 m=2 cm. A total of 152 000 elements were analyzed.

### 2.3.3. Boundary and Initial conditions

The “inlet” surface where the water enters the flow volume is defined as the “mass flow inlet”. Mass flow inlet is determined in kg/s, that is, lt/sn. The “outlet” surface of the flow volume is defined as the “pressure outlet”. Air and water can come out freely from the outlet surface (Fig 9). The k-omega RNG was used as the turbulence model. In the experiments carried out in the laboratory, there is a free surface water flow and atmospheric pressure on it. Therefore, analysis is designed as a 2-phase flow so that both air and water can be found in the flow volume. The “Multiphase” model was chosen as the VOF (Volume of Fluid) method to provide the two-phase flow. The effect of air on water (atmospheric pressure) is also considered in this way . To make the solution more detailed, an "explicit" solution was used instead of an "implicit" solution. In the analysis, a solution was made according to the variable flow (Transient Flow). In the analysis, “time step size” varies between 0.001 sec and 0.005 sec depending on the height of the weirs and the flow rate.

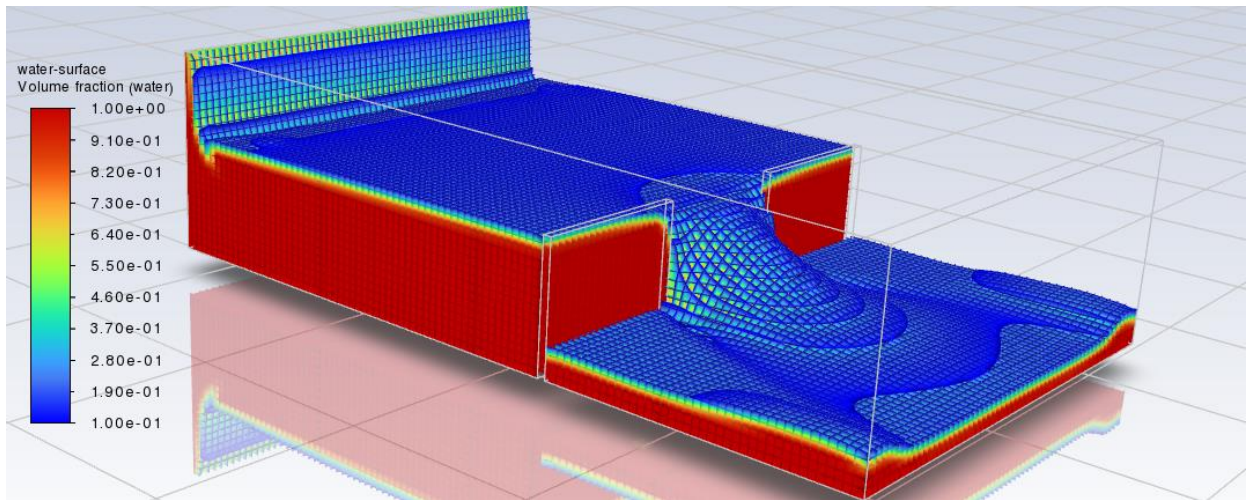


Fig 9: 3D view of the numerical result

### 3. Results

To determine the hydraulic performance of 2 spurs placed opposite each other in the open channel system, experiments were carried out at two different flow rates which are  $Q=17.66$  lt/s and  $Q=15.27$  lt/s. While the water depth in the upstream part of the spurs is  $H_T=14.40$  cm for a flow rate of  $Q=17.66$  lt/s, the water depth is  $H_T=13.40$  cm for a flow rate of  $Q=15.27$  lt/sec. For each flow rate value,  $V_x$ ,  $V_y$  and  $V_z$  velocities in the X, Y and Z axis were measured with the ADV device at 20 different points indicated in the Fig 6. above. For both flow rates, the flow does not overtop the spurs and is in free flow condition. In addition, numerical models were created for both flow rates and 3-axis velocity readings were made from these models at the same point in the experiments (Fig 10).

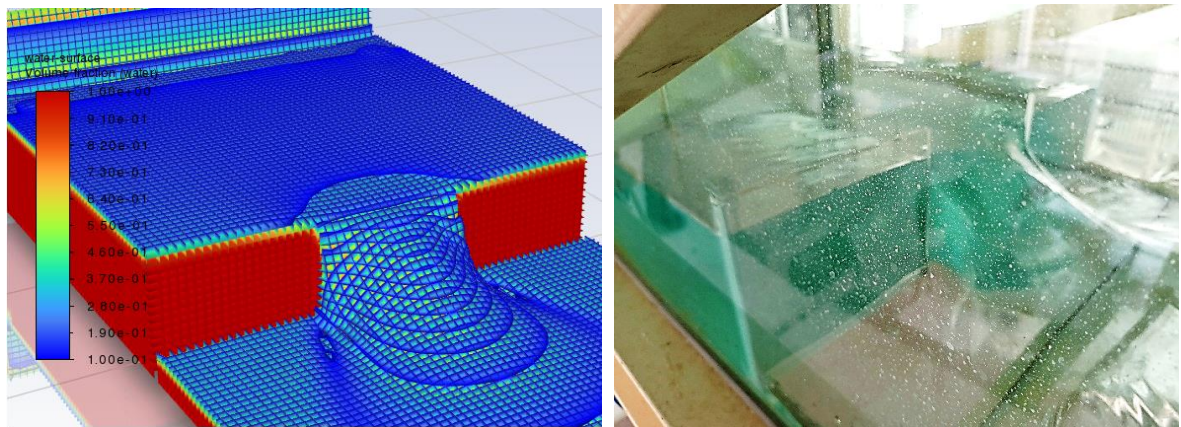


Fig 10: Comparison of the numerical and experimental model

Before comparing the numerical model with the velocity data obtained from the experiments, the similarity of the numerical model and the physical experimental setup was checked. The numerical model gave  $H_T=14.30$  cm and  $H_T=13.35$  cm flow depth values for  $Q=17.66$  lt/sn and  $Q=15.27$  lt/sn flow rates, respectively. When the 3D view obtained from the numerical model are compared with the experiments, the profile and water surfaces formed by the flow as it passes through the spurs are extremely similar. The velocity results obtained from the experiments and numerical models to determine the effects of the spurs on the flow and the flow patterns they cause on the upstream side are given in the below for each flow rate value. Since the current moves towards the spurs and to analyze the current movement more accurately, the velocities are ordered in the direction of the flow.

**Table 1: V<sub>x</sub>, V<sub>y</sub> and V<sub>z</sub> velocity Result obtained from numeral and experimental model.**

Experimental					Numerical				
Velocity measurements for Q=17.66 lt/sn					Velocity measurements for Q=17.66 lt/sn				
	1A	2A	3A	4A		1A	2A	3A	4A
V <sub>x</sub>	21.00	21.29	21.91	19.72	V <sub>x</sub>	21.42	22.17	20.02	19.27
V <sub>y</sub>	0.90	-0.48	-3.03	-7.25	V <sub>y</sub>	0.50	-0.50	-3.45	-7.87
V <sub>z</sub>	0.45	0.78	1.02	2.08	V <sub>z</sub>	0.67	0.83	1.31	2.46
	1B	2B	3B	4B		1B	2B	3B	4B
V <sub>x</sub>	22.22	23.66	22.46	25.45	V <sub>x</sub>	22.41	23.25	26.14	28.93
V <sub>y</sub>	-0.65	-1.44	-4.41	-8.95	V <sub>y</sub>	-0.52	-1.61	-4.01	-8.45
V <sub>z</sub>	-0.03	-0.15	0.29	-0.22	V <sub>z</sub>	0.05	0.11	0.20	0.32
	1C	2C	3C	4C		1C	2C	3C	4C
V <sub>x</sub>	21.05	24.24	25.11	33.20	V <sub>x</sub>	22.50	25.12	28.33	36.73
V <sub>y</sub>	-1.30	-0.52	-0.31	-0.41	V <sub>y</sub>	-0.59	-0.65	-0.88	-0.47
V <sub>z</sub>	0.22	-0.67	-1.23	-1.55	V <sub>z</sub>	0.16	-0.78	-1.42	-3.80
	1D	2D	3D	4D		1D	2D	3D	4D
V <sub>x</sub>	21.79	22.14	22.38	27.12	V <sub>x</sub>	21.84	22.64	26.37	28.56
V <sub>y</sub>	0.32	1.14	3.39	9.92	V <sub>y</sub>	0.39	1.66	4.75	8.83
V <sub>z</sub>	0.16	0.47	0.33	-0.85	V <sub>z</sub>	0.19	0.24	0.33	-0.15
	1E	2E	3E	4E		1E	2E	3E	4E
V <sub>x</sub>	21.26	21.29	19.00	18.50	V <sub>x</sub>	21.57	21.48	19.84	19.12
V <sub>y</sub>	0.23	1.01	3.31	6.30	V <sub>y</sub>	0.20	1.02	3.52	7.17
V <sub>z</sub>	0.49	0.65	0.93	2.09	V <sub>z</sub>	0.73	0.91	1.26	2.35

Experimental					Numerical				
Velocity measurements for Q=15.27 lt/sn					Velocity measurements for Q=15.27 lt/sn				
	1A	2A	3A	4A		1A	2A	3A	4A
V <sub>x</sub>	20.30	20.75	17.84	13.20	V <sub>x</sub>	20.83	21.20	19.38	14.50
V <sub>y</sub>	-0.53	-1.89	-3.65	-7.99	V <sub>y</sub>	-0.42	-2.03	-4.10	-8.25
V <sub>z</sub>	-0.39	0.21	0.85	1.82	V <sub>z</sub>	-0.22	0.42	1.02	1.93
	1B	2B	3B	4B		1B	2B	3B	4B
V <sub>x</sub>	21.77	21.76	22.36	24.99	V <sub>x</sub>	22.03	22.25	23.41	25.41
V <sub>y</sub>	0.17	-0.95	-2.52	-10.84	V <sub>y</sub>	-0.42	-1.03	-2.64	-11.89
V <sub>z</sub>	-0.22	-0.35	0.35	0.32	V <sub>z</sub>	0.09	0.18	0.34	0.22
	1C	2C	3C	4C		1C	2C	3C	4C
V <sub>x</sub>	20.05	20.60	24.11	32.25	V <sub>x</sub>	21.06	22.30	24.94	32.00
V <sub>y</sub>	1.17	-0.37	0.08	0.54	V <sub>y</sub>	0.65	-0.24	0.12	-0.35
V <sub>z</sub>	-0.21	-0.39	-0.84	-1.37	V <sub>z</sub>	-0.11	-0.65	-0.87	-2.01
	1D	2D	3D	4D		1D	2D	3D	4D
V <sub>x</sub>	19.74	19.71	18.79	22.56	V <sub>x</sub>	19.20	20.01	21.13	22.80
V <sub>y</sub>	1.14	0.91	4.04	9.21	V <sub>y</sub>	0.92	1.85	4.52	9.45
V <sub>z</sub>	0.63	0.25	0.57	0.91	V <sub>z</sub>	0.12	0.24	-0.42	0.45
	1E	2E	3E	4E		1E	2E	3E	4E
V <sub>x</sub>	19.97	19.89	17.78	13.81	V <sub>x</sub>	20.23	20.47	19.84	14.72
V <sub>y</sub>	2.56	2.04	4.38	9.43	V <sub>y</sub>	1.93	2.74	4.12	9.01
V <sub>z</sub>	0.46	-0.11	0.03	1.02	V <sub>z</sub>	-0.29	0.35	1.53	1.89

When the measurement points are examined, these points are symmetrical with respect to the C axis in the direction of the flow. At the same flow rate, A - E axis and B - D axis velocity values should be close. When the values given in the Table 1 are examined, these axes gave velocity values close to each other, this shows that the experiments were carried out correctly and the velocities were measured correctly. When the numerical model is compared with the experimental data, it is seen that the velocity values are extremely close. For example, when comparing the experimental and numerical results at point 4B, the numerical model has a 3 cm/sn higher horizontal

$V_x$  velocity. As with the horizontal velocity at point 4B, the numerical model can give a velocity less than 0.5 cm/sn. The main reason for these speed differences is the size of the mesh used. For more detailed results, it is necessary to use mesh in smaller sizes. When the values in the Table 1 are examined in general, the maximum difference between the numerical and experimental models does not exceed % 9 percentage. No eddy structure was observed behind the spurs. The point where the velocity is lowest behind the spurs is at the junction of the spurs with the wall on the upstream surface. At these points, no measurement was made with the ADV device, but according to the data obtained from the numerical model, the total speed decreases by  $V_m=3.2$  cm/s. The highest velocity value reached by the flow is at the exit point between the spurs. At this point, the speed reaches up to  $V_m=88$  cm/s. General velocity distributions and streamlines are shown in the Fig 11.

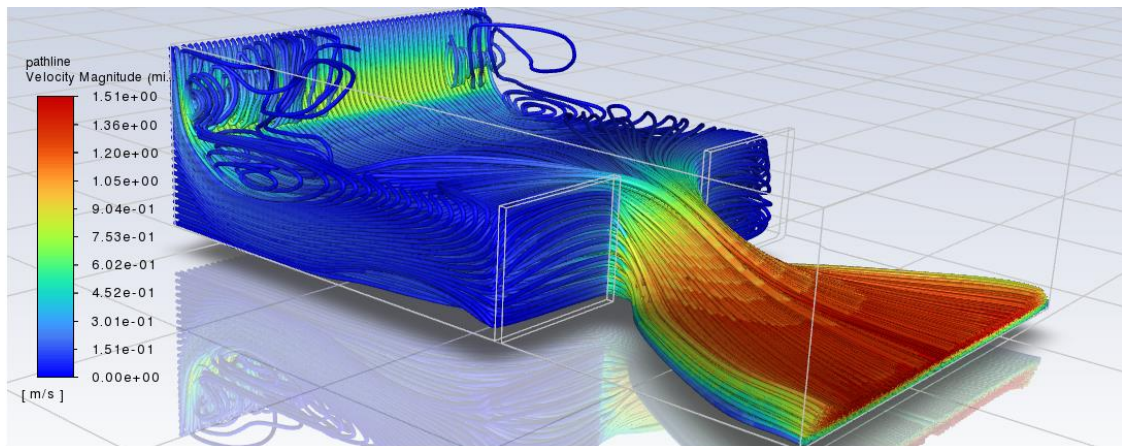


Fig 11: Flow patterns and velocity distribution around the spurs

The results obtained in this study were evaluated separately for the velocities of  $V_x$ ,  $V_y$  and  $V_z$  on the axis. For  $V_x$  speeds, while a decrease in  $V_x$  velocities was observed in the A and E axis as the flow approached the spurs, an increase was observed in  $V_x$  velocities in the B, C and D axis. The increase in velocity  $V_x$  in the C axis is greater than the velocity in the B and D axis. The reason for the slowdown in velocities in the A and E axis is that the current encounters the spur walls and the current is directed towards the spur gap. When the  $V_x$  velocities in the 1 axis are compared, the velocities are close, but the highest velocity value in the 4 axis occurs in the C axis. While the  $V_x$  velocity in the C axis is 26% higher than the B and D axis, it is 90% higher than the  $V_x$  velocity in the A and E axis. Numerical models gave results consistent with experiments. Fig 12 taken from the numerical model to support the data in the experiments are given below. In the numerical model, while the  $V_x$  velocities decrease in the A and E axis, the velocities increase in the B, C and D axis.

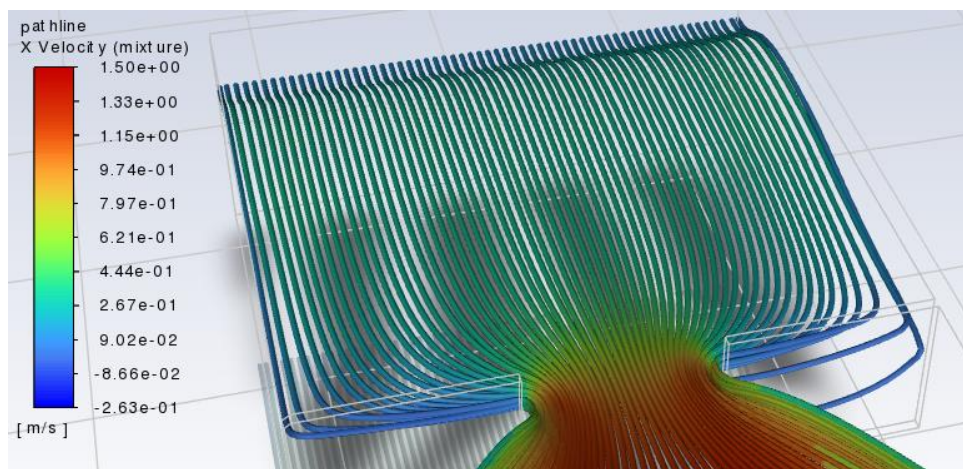


Fig 12: Velocity distribution in X axis

In the A and B axis,  $V_y$  values increasing in magnitude in the -Y axis direction as the current approaches the spurs, while  $V_y$  velocities increasing in magnitude in the +Y direction from the D and E axis were observed in the same way. In sections 2 and 3, the amount of increase in  $V_y$  velocities in the B and D axis is less than the increase in the  $V_y$  values in the A and E axis. In previous studies, for  $V_z$  speeds in cases where the spurs were placed on one side of the channel, the flow showed a downward movement after hitting the spur wall, whereas in these experiments the flow moves upwards. This upward movement is seen in the  $V_z$  velocities in the 4 axes (A, B, D and E). The positive velocities  $V_z$  indicate that the cohesive current upstream of the spur walls is upstream. As the current approaches the spurs, the velocities in the z axis increase. The velocity in the Z axis is in the upward direction (Fig 13). When the results obtained from this study on spurs are compared with previous studies, the most important differences in the results are flow patterns of the steam and vortex structures on the upstream surface of the spurs. In previous studies where spurs were placed on one side of the channel [21], the flow hitting the upstream surface of the spur followed a downward movement, whereas in this study the flow followed an upward movement. In addition, in cases where spurs are placed unilaterally, vortex structures are formed on the upstream and downstream sides of the spurs [14], whereas no vortex structure was formed in this study.

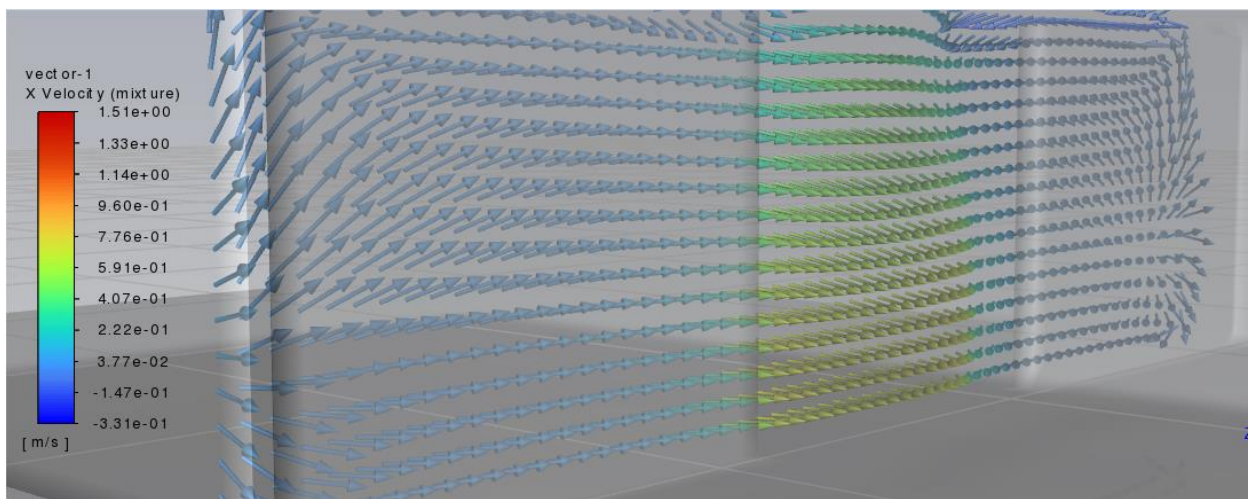


Fig 13: Upward  $V_z$  velocities in the flow that facing the spur wall.

#### 4. Conclusions

By placing the spurs in an open channel, scours occur before and after the spurs due to changes in flow conditions and velocities. Determination of velocity distributions around the spur accurately is extremely important for spur design. For a sustainable and hydraulically efficient spur design, flow velocities, flow conditions, sediment characteristics and stream morphology around the spur should be well investigated. As a result of the experiments conducted on two spurs placed opposite each other in an open channel system, it was observed that the velocity of the streamlines changed significantly with the change of the flow rate value, but the general flow pattern of the streamlines remained the same. The velocity data obtained from the numerical model gave close results with the experimental data. In this study, unlike previous studies, spurs were placed on both sides of the channel. The hydraulic behavior of spurs placed in both sides, show significantly different flow patterns, vortices, and velocities from that of single-sided spurs. In addition, numerical models provided a detailed view of streamlines that could not be obtained from experiments.

#### 5. Nomenclature

$V_x$	X velocity
$V_y$	Y velocity
$V_z$	Z velocity
$V_m$	Total velocity magnitude
$Q$	Discharge

## References

- [1] H. Zhang, H. Nakagawa, Investigation on Morphological Consequences of Spur Dyke with Experimental and Numerical Methods, 2008.
- [2] A. Moradinejad, M. Saneie, A. Ghaderi, S. M. Zamanieh Shahri, Experimental study of flow pattern and sediment behavior near the intake structures using the spur dike and skimming wall, *Applied Water Science*, Vol. 9, No. 8, pp. 1-11, 2019/11//, 2019.
- [3] M. M. Alemu, M. M. Alemu, Integrated Watershed Management and Sedimentation, *Journal of Environmental Protection*, Vol. 7, No. 4, pp. 490-494, 2016/3//, 2016.
- [4] A. Yıldız, A. İ. Martı, M. Göğüş, Numerical and experimental modelling of flow at Tyrolean weirs, *Flow Measurement and Instrumentation*, Vol. 81, pp. 102040-102040, 2021/10//, 2021.
- [5] C. Gisonni, W. H. Hager, Spur Failure in River Engineering, *Journal of Hydraulic Engineering*, Vol. 134, No. 2, pp. 135-145, 2008/2//, 2008.
- [6] M. Pandey, Z. Ahmad, P. K. Sharma, Scour around impermeable spur dikes: a review, <https://doi.org/10.1080/09715010.2017.1342571>, Vol. 24, No. 1, pp. 25-44, 2017/1//, 2017.
- [7] M. Alauddin, M. M. Hossain, M. N. Uddin, M. E. Haque, A Review on Hydraulic and Morphological Characteristics in River Channels Due to Spurs, 2017/8//, 2017.
- [8] A. Safarzadeh, S. A. A. S. Neyshabouri, A. R. Zarrati, Experimental Investigation on 3D Turbulent Flow around Straight and T-Shaped Groynes in a Flat Bed Channel, *Journal of Hydraulic Engineering*, Vol. 142, No. 8, pp. 04016021-04016021, 2016/4//, 2016.
- [9] K. Hosseinzadeh, S. Roghani, A. R. Mogharrebi, A. Asadi, D. D. Ganji, Optimization of hybrid nanoparticles with mixture fluid flow in an octagonal porous medium by effect of radiation and magnetic field, *Journal of Thermal Analysis and Calorimetry*, Vol. 143, No. 2, pp. 1413-1424, 2021/1//, 2021.
- [10] A. K. Rostami, K. Hosseinzadeh, D. D. Ganji, Hydrothermal analysis of ethylene glycol nanofluid in a porous enclosure with complex snowflake shaped inner wall, <https://doi.org/10.1080/17455030.2020.1758358>, Vol. 32, No. 1, pp. 1-18, 2020.
- [11] C. Özyaman, C. Yerdelen, E. Eris, R. Daneshfaraz, Experimental investigation of scouring around a single spur under clear water conditions, *Water Supply*, Vol. 22, No. 3, pp. 3484-3497, 2022/3//, 2022.
- [12] M. Koken, M. Gogus, Effect of spur dike length on the horseshoe vortex system and the bed shear stress distribution, <https://doi.org/10.1080/00221686.2014.967819>, Vol. 53, No. 2, pp. 196-206, 2014/3//, 2014.
- [13] A. N. Giglou, J. A. McCorquodale, L. Solari, Numerical study on the effect of the spur dikes on sedimentation pattern, *Ain Shams Engineering Journal*, Vol. 9, No. 4, pp. 2057-2066, 2018/12//, 2018.
- [14] J. Ning, G. Li, S. Li, Numerical Simulation of the Influence of Spur Dikes Spacing on Local Scour and Flow, *Applied Sciences 2019*, Vol. 9, Page 2306, Vol. 9, No. 11, pp. 2306-2306, 2019/6//, 2019.
- [15] K. Sharma, P. K. Mohapatra, Separation Zone in Flow past a Spur Dyke on Rigid Bed Meandering Channel, *Journal of Hydraulic Engineering*, Vol. 138, No. 10, pp. 897-901, 2012/3//, 2012.
- [16] M. Koken, Coherent structures around isolated spur dikes at various approach flow angles, <http://dx.doi.org/10.1080/00221686.2011.616316>, Vol. 49, No. 6, pp. 736-743, 2011/12//, 2011.
- [17] M. A. Imran, A. Shaheen, E. S. M. Sherif, M. Rahimi-Gorji, A. H. Seikh, Analysis of peristaltic flow of Jeffrey six constant nano fluid in a vertical non-uniform tube, *Chinese Journal of Physics*, Vol. 66, pp. 60-73, 2020/8//, 2020.
- [18] D. F. Jamil, S. Saleem, R. Roslan, F. S. Al-Mubaddel, M. Rahimi-Gorji, A. Issakhov, S. U. Din, Analysis of non-Newtonian magnetic Casson blood flow in an inclined stenosed artery using Caputo-Fabrizio fractional derivatives, *Computer Methods and Programs in Biomedicine*, Vol. 203, pp. 106044-106044, 2021/5//, 2021.
- [19] M. Hassan, E. R. El-Zahar, S. U. Khan, M. Rahimi-Gorji, A. Ahmad, Boundary layer flow pattern of heat and mass for homogenous shear thinning hybrid-nanofluid: An experimental data base modeling, *Numerical Methods for Partial Differential Equations*, Vol. 37, No. 2, pp. 1234-1249, 2021/3//, 2021.
- [20] K. G. Kumar, M. G. Reddy, P. Vijaya kumari, A. Aldalbahi, M. Rahimi-Gorji, M. Rahaman, Application of different hybrid nanofluids in convective heat transport of Carreau fluid, *Chaos, Solitons & Fractals*, Vol. 141, pp. 110350-110350, 2020/12//, 2020.
- [21] M. Koken, G. Constantinescu, An investigation of the flow and scour mechanisms around isolated spur dikes in a shallow open channel: 1. Conditions corresponding to the initiation of the erosion and deposition process, *Water Resources Research*, Vol. 44, No. 8, pp. 8406-8406, 2008/8//, 2008.